Sensors and Materials, Vol. 30, No. 3 (2018) 515–523
MYU Tokyo

S & M 1514

Effects of Aging Treatment on Microstructure of High-Al-content Fe-15Mn-10Al-1.0C Alloy

Wei-Chih Chen,[1*] Chung-Chun Wu,[2] and Wei-Yang Chang[2]

[1]Electrical and Mechanical Technology Department, Southern Taiwan University of Science and Technology, No. 1, Nantai St., Yongkang Dist., Tainan City 710, Taiwan, R.O.C.
[2]Mechanical Engineering Departments, Southern Taiwan University of Science and Technology, No. 1, Nantai St., Yongkang Dist., Tainan City 710, Taiwan, R.O.C.

(Received July 29, 2017; accepted November 2, 2017)

Keywords: Fe-Mn-Al-C alloy, B_2 and $D0_3$ ordered phases, spinodal decomposition

The purpose of this study is to examine the effects of aging treatment on the microstructures of the dual-phase Fe-15Mn-10Al-1.0C alloy by optical microscopy (OM) and transmission electron microscopy (TEM). On the basis of the results of our experiments, we reached the following conclusions. Under the as-quenched condition, the microstructure of the Fe-15Mn-10Al-1.0C alloy was a mixture of ferrite and austenite phases. TEM examination revealed that (Fe,Mn)3AlC$_X$ carbides precipitated within the austenite matrix, and (B_2 + $D0_3$) ordered phases could be found within the ferrite region owing to the mechanism of the $\alpha \rightarrow \alpha + B_2 \rightarrow \alpha + D0_3$ ordering transition. This result indicated that an increase in the amount of Al added to the Fe-Mn-Al-C alloy would enhance both the formation of ordered phases within the ferrite matrix and the precipitation of κ-carbides within the austenite matrix. When the alloy was aged at 650 °C for 24 h, phase decomposition of $\gamma \rightarrow \kappa' + B_2$ was observed on the austenite grain boundary.

1. Introduction

Recently, Fe-Mn-Al-C alloys have been successfully developed for some specialized applications, such as high-strength alloy plates, cold-rolled plates, alloy bars, metal inert gas (MIG) welding wires, high-temperature furnace strips, golf clubs, and precision industrial castings. Several patents concerning Fe-Mn-Al-C alloys have been granted, indicating that the Fe-Mn-Al-C alloys have great potential for specific applications.[1–4]

A considerable amount of interest has focused on the effects of various alloying elements and of aging conditions on the microstructure changes and mechanical properties of Fe-Mn-Al-C alloys. To date, most examinations have been focused on the effects of Si, Ti, Mo, Cu, Nb, Ni, and Cr additions as well as the different aging processes in the Fe-Mn-Al-C alloy. However, there has been little investigation into the effects of aging treatment on high-Al-content Fe-Mn-Al-C alloy. Therefore, the purpose of this study is to examine the effects of aging treatment on the microstructure and mechanical properties of the Fe-15Mn-10Al-1.0C alloy by transmission electron microscopy (TEM).[5–8]

*Corresponding author: e-mail: da0z0201@stust.edu.tw
http://dx.doi.org/10.18494/SAM.2018.1759

ISSN 0914-4935

2. Experimental Procedures

Fe-15Mn-10Al-1.0C alloy ingots were prepared in an air induction furnace. After being homogenized at 1200 °C for 24 h, the ingots were hot-forged and then cold-rolled to a final thickness of 30 mm. The sheets were subsequently solution-heat-treated at 1050 °C for 1 h and rapidly quenched in room-temperature water. The aging processes were carefully performed at temperatures ranging from 450 to 750 °C for various durations in salt baths and then the ingots were quenched in water.

Specimens for TEM were prepared by means of a double-jet electrolyte of 10% perchloric acid, 30% acetic acid, and 60% ethanol. The polishing temperature was kept in the range from −10 to 0 °C, and the current was kept in the range of 30 to 40 mA. Electron microscopy was performed using a Philips FEG-20 scanning transmission electron microscope (STEM) operating at 200 kV.

3. Results and Discussion

Under the as-quenched condition, the microstructure of the Fe-15Mn-10Al-1.0C alloy was a mixture of ferrite and austenite phases, as shown in Fig. 1(a). When comparing Fe-15Mn-8Al-1.0C alloy and Fe-15Mn-10Al-1.0C alloy under the as-quenched condition, it was found that the Fe-15Mn-8Al-1.0C alloy was a mixture of only austenite phases, as shown in Fig. 1(b), because an increase in the amount of Al in the Fe-Mn-Al-C alloy causes ferrite phase stabilization. The microstructure was further observed by TEM. Figures 2 and 3 are electron micrographs of the Fe-15Mn-10Al-1.0C alloy under the as-quenched condition. Figure 2(a) is the selected area diffraction pattern (SADP) of the austenite matrix, where the foil normal is [001], and it shows the existence of austenite matrix diffraction spots and the precipitate of κ-carbide diffraction spots. Figure 2(b) is the dark-field (DF) electron micrograph of the (100) κ-carbide precipitate spot in Fig. 2(a), revealing the precipitation of $(Fe,Mn)^3AlC_X$ carbides having a L'12 crystal structure, which could be observed within the austenite matrix.[3–5] Figures 3(a) and 3(b) are the SADPs of the ferrite region, where the foil normals are [001] and [011], respectively, showing

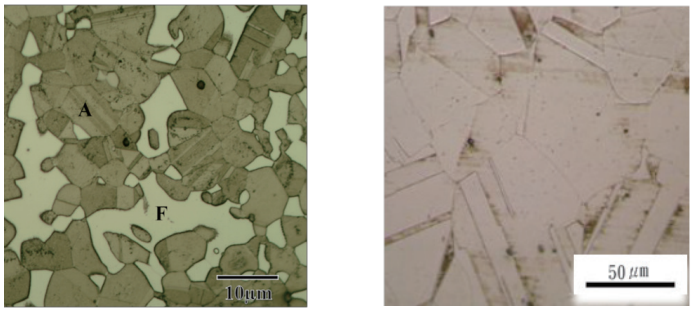

(a) (b)

Fig. 1. (Color online) Optical micrograph of Fe-Mn-Al-C alloys after solution heat treatment at 1050 °C for 1 h. (a) Fe-15Mn-10Al-1.0C and (b) Fe-15Mn-8Al-1.0C.

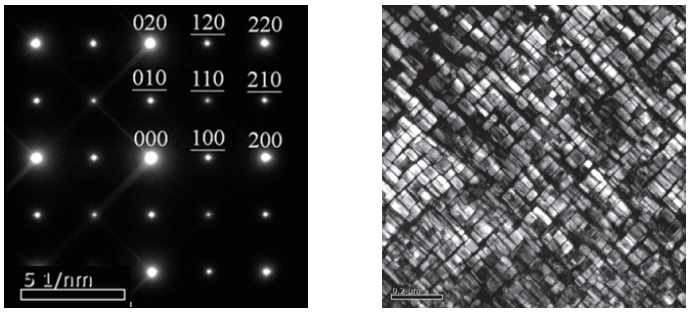

(a) (b)

Fig. 2. TEM images of Fe-15Mn-10Al-1.0C alloy under the as-quenched condition. (a) SADP of the austenite matrix. The foil normal is [001]. (b) (100) κ-carbide DF electron micrograph.

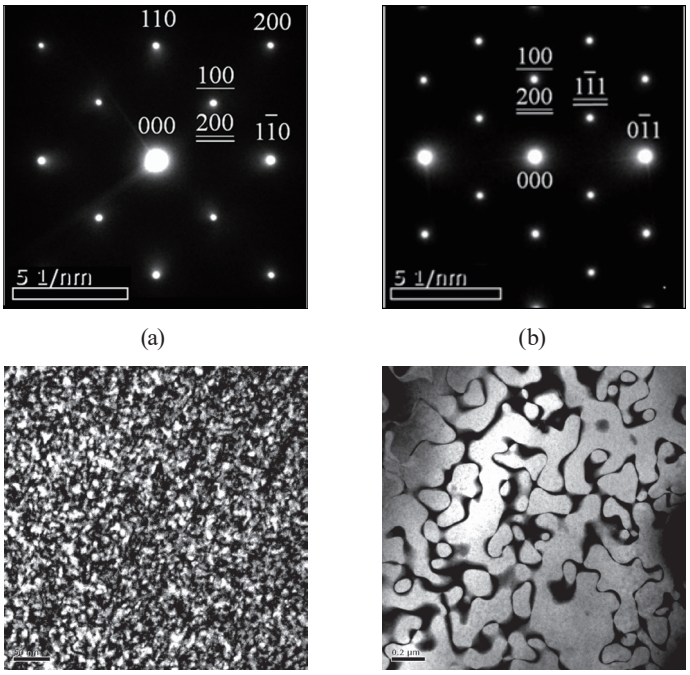

(a) (b)

(c) (d)

Fig. 3. TEM images of Fe-15Mn-10Al-1.0C alloy under the as-quenched condition. SADPs of the ferrite matrix where (a) the foil normal is [001] and (b) the foil normal is [011]. DF electron micrographs of (c) the (111) $D0_3$ phase and (d) the (200) $D0_3$ and (100) B_2 phases.

the existence of ferrite matrix diffraction spots and the precipitate of B_2 and $D0_3$ diffraction spots. Figure 3(c) is the DF electron micrograph of the (111) $D0_3$ spot in Fig. 3(a), showing the existence of a tiny $D0_3$ ordered phase. Figure 3(d) is the DF electron micrograph of the (200) $D0_3$ and (100) B_2 spots in Fig. 3(b), showing the existence of $D0_3$ and B_2 phases. When we compare Figs. 3(c) and 3(d), we find that the B_2 phase is larger than the $D0_3$ phase because the B_2 phase is more stable at high temperature. Additionally, the $D0_3$ phase precipitates during quenching. The experimental results indicated that the B_2 and $D0_3$ ordered phases are found within the ferrite owing to the $\alpha \rightarrow \alpha + B_2 \rightarrow \alpha + D0_3$ ordering transition mechanism. This

result indicated that an increase in the amount of Al in the Fe-Mn-Al-C alloy would enhance both the formation of ordered phases with the ferrite matrix and the precipitation of κ-carbides within the austenite matrix.[7,8]

Figures 4 and 5 are TEM images of the Fe-15Mn-10Al-1.0C alloy aged at 450 °C for 24 h. Figure 4(a) is the SADP of the austenite matrix and the foil normal is [011]. It shows the existence of austenite matrix diffraction spots and the precipitate of κ-carbide diffraction spots. Figure 4(b) is the DF electron micrograph of the (100) κ-carbide spots in Fig. 4(a), showing the well-grown and newly precipitated $(Fe,Mn)^3AlC_X$ carbides with L'12 crystal structures and

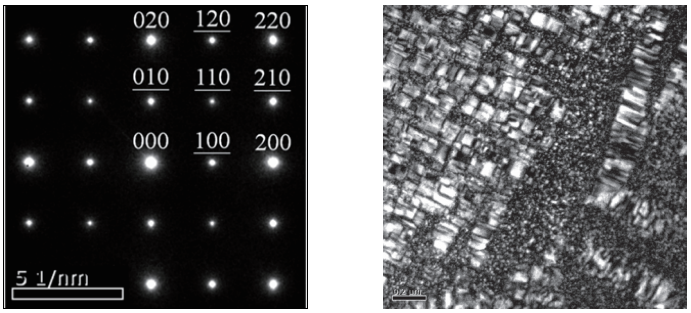

(a) (b)

Fig. 4. TEM images of Fe-15Mn-10Al-1.0C alloy aged at 450 °C for 24 h. (a) SADP of the austenite matrix. The foil normal is [001]. (b) (100) κ-carbide DF electron micrograph.

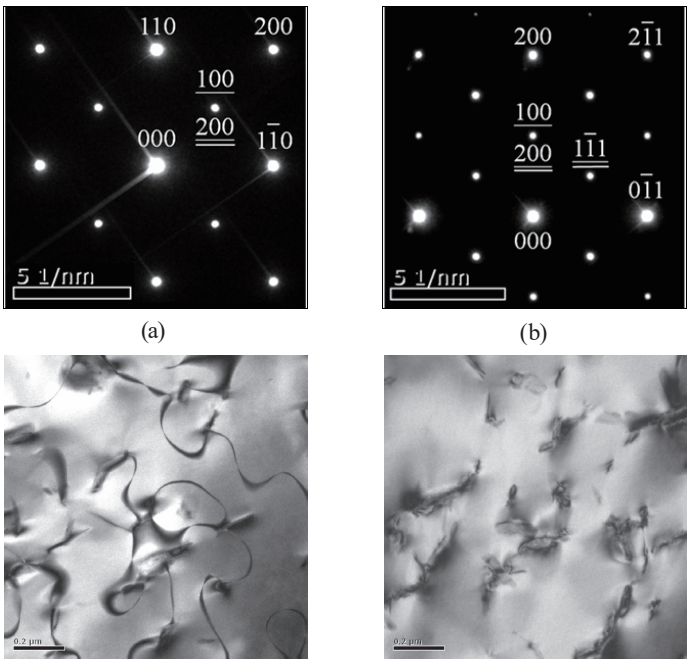

(a) (b)

(c) (d)

Fig. 5. TEM images of Fe-15Mn-10Al-1.0C alloy aged at 450 °C for 24 h. SADPs of the ferrite matrix where (a) the foil normal is [001] and (b) the foil normal is [011]. DF electron micrographs of (c) the (111) $D0_3$ phase and (d) the (200) $D0_3$ and (100) B_2 phases.

different morphologies within the austenite matrix. Figures 5(a) and 5(b) are SADPs of the ferrite region and the foil normals are [001] and [011], respectively. They show the existence of ferrite matrix diffraction spots and the B_2 and $D0_3$ precipitate diffraction spots. Figures 5(c) and 5(d) are DF electron micrographs of the (111) $D0_3$ and (100) B_2 + (200) $D0_3$ spots in Figs. 5(a) and 5(b), respectively. These show that the growth of the $D0_3$ ordered phase within the ferrite region is stable, with different morphologies of (α + $D0_3$) phases within the ferrite region.

Figures 6(a) and 6(b) are TEM images of the Fe-15Mn-10Al-1.0C alloy that was aged at 550 ℃ for 24 h. Figure 6(a) is the DF electron micrograph of the (100) κ-carbide spot within the austenite matrix, revealing the precipitation of κ-carbides with an L'12 crystal structure within the austenite matrix. Figure 6(b) is a DF electron micrograph of the (111) $D0_3$ spot within the ferrite matrix, showing the existence of only the $D0_3$ phase. No B_2 phase within the ferrite matrix could be observed. It can be seen that the stable temperature of the $D0_3$ phase is below approximately 550 ℃.

Figure 7(a) is an optical micrograph of the Fe-15Mn-10Al-1.0C alloy aged at 650 ℃ for 24 h, which shows the austenite phase decomposition. Figure 7(b) is a bright-field (BF) electron micrograph of the austenite grain boundary, showing rod-like κ'-carbides within both the austenite grain boundary and the ferrite mixture. Figure 7(c) is the SADP electron micrograph of the region marked P near the carbides, showing the existence of ferrite matrix diffraction spots and the precipitate of B_2 and $D0_3$ diffraction spots. Figure 7(d) is the DF electron micrograph of the (111) $D0_3$ spot in Fig. 7(c). It shows that in the Fe-15Mn-10Al-1.0C alloy aged at 650 ℃ for 24 h, phase decomposition of $\gamma \rightarrow \kappa' + B_2$ could be observed on the austenite grain boundary. It is worth noting that the $\gamma \rightarrow \kappa' + B_2$ transformation was quite different from the $\gamma \rightarrow \alpha + \kappa'$, $\gamma \rightarrow \kappa' + D0_3$, and $\gamma \rightarrow \kappa' + \beta$-Mn transformations observed by others. Figures 8(a) and 8(b) are TEM images of the Fe-15Mn-10Al-1.0C alloy aged at 600 ℃ for 24 h. Figures 8(a) and 8(b) are the DF electron micrographs of the $D0_3$ and B_2 + $D0_3$ spots within the ferrite mixture, showing the growth of the B_2 phase within the ferrite mixture but the beginning of $D0_3$ phase decomposition. Figures 9(a) and 9(b) are DF electron micrographs of the Fe-15Mn-10Al-1.0C alloy aged at 650 ℃ for 24 h, which show tiny $D0_3$ phases and B_2 phases within the ferrite mixture. It can be seen that the transition temperature of the $B_2 \rightarrow \alpha$ + $D0_3$ ordered transformation was found to be within the narrow range of 600–650 ℃, which was quite

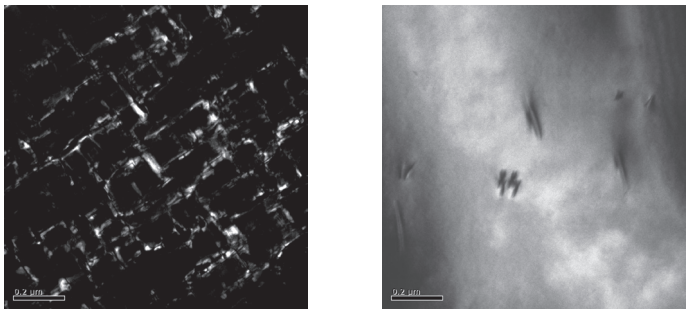

(a) (b)

Fig. 6. TEM images of the Fe-15Mn-10Al-1.0C alloy aged at 550 ℃ for 24 h. DF electron micrographs of (a) the (100) κ-carbide and (b) the (111) $D0_3$ phase.

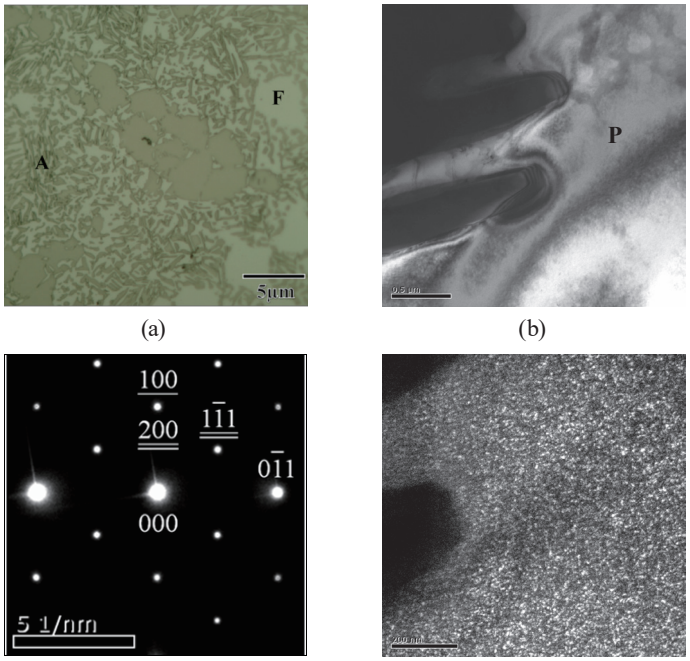

(a) (b)

(c) (d)

Fig. 7. (Color online) Fe-15Mn-10Al-1.0C alloy aged at 650 °C for 24 h. (a) Optical micrograph. (b) BF electron micrograph. (c) SADP of the region marked as P. The foil normal is [001]. (d) (100) κ-carbide DF electron micrograph.

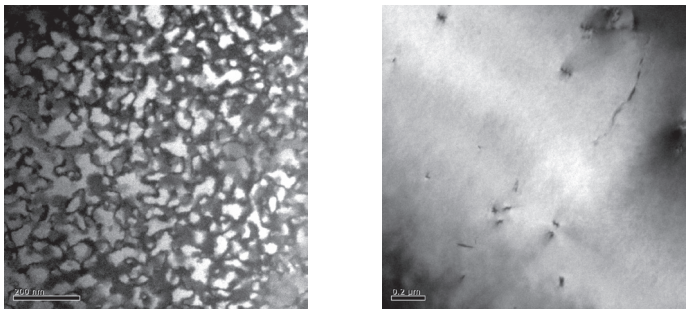

(a) (b)

Fig. 8. TEM images of the Fe-15Mn-10Al-1.0C alloy aged at 600 °C for 24 h. DF electron micrographs of (a) the (111) $D0_3$ phase and (b) the (200) $D0_3$ and (100) B_2 phases.

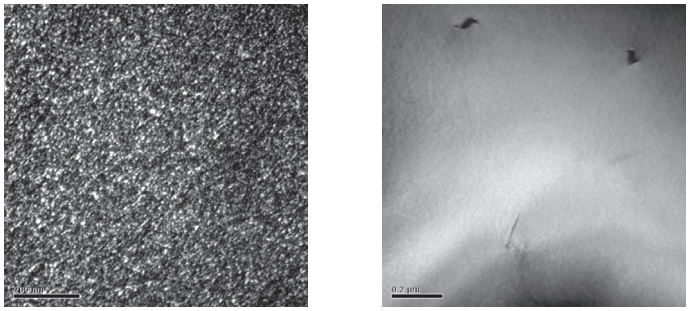

(a) (b)

Fig. 9. TEM images of the Fe-15Mn-10Al-1.0C alloy aged at 650 °C for 24 h. DF electron micrographs of (a) the (111) $D0_3$ phase and (b) the (200) $D0_3$ and (100) B_2 phases.

different from the $\alpha \rightarrow B_2 \rightarrow \alpha + D0_3$ transition previously observed in the Fe-Mn-Al-C alloy by other researchers.

Figure 10 is an optical micrograph of the Fe-15Mn-10Al-1.0C alloy aged at 750 ℃ for 24 h, showing the austenite phase decomposition. The microstructure was further observed using a TEM. Figures 11(a) and 11(b) are TEM images of the Fe-15Mn-10Al-1.0C alloy aged at 750 ℃ for 24 h. Figure 11(a) is a BF electron micrograph of the area mixed austenite and ferrite. Figure 11(b) is the SADP of the austenite matrix and the foil normal is [011]. It shows the existence of only austenite matrix diffraction spots; no precipitate of κ-carbide diffraction spots could be observed. It can be seen that the κ-carbide stability growth temperature range is 450–750 ℃, but under the as-quenched condition, the existence of κ-carbide within the austenite matrix could be observed. Figures 12(a) and 12(b) show energy dispersive X-ray spectroscopy (EDS) spectra obtained from the austenite matrix of the Fe-15Mn-10Al-1.0C alloy aged at 750 ℃ for 24 h and from the austenite matrix of the Fe-15Mn-10Al-1.0C alloy under the as-quenched condition, respectively. The difference between these two EDS spectra could be caused by the presence of manganese. It is clear that austenite matrix of the alloy under the as-quenched condition is manganese-rich and has a manganese-to-aluminum ratio of 3:1, which is confirmed by electron diffraction analysis. According to Ref. 5, this result is caused by the κ-carbide precipitation by spinodal decomposition during quenching.

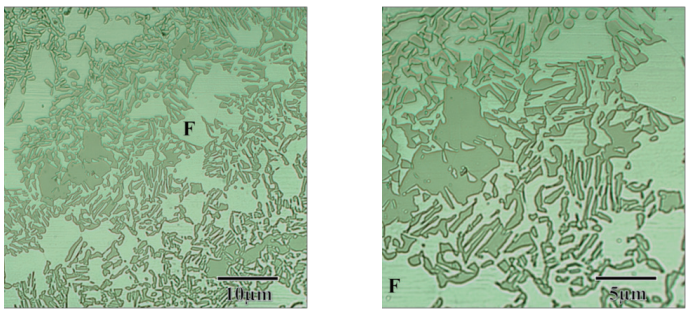

(a) (b)

Fig. 10. (Color online) Optical micrograph of the Fe-15Mn-10Al-1.0C alloy aged at 750 ℃ for 24 h. (a) 100× and (b) 500×.

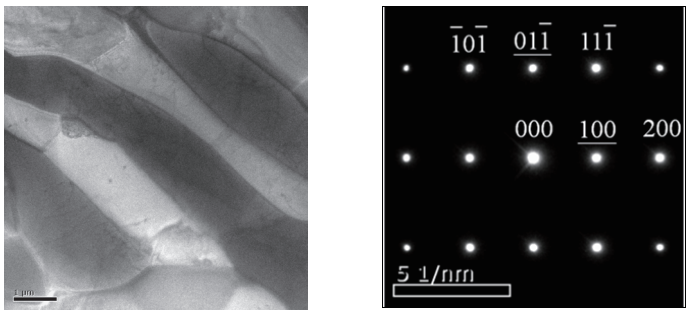

(a) (b)

Fig. 11. TEM images of the Fe-15Mn-10Al-1.0C alloy aged at 750 ℃ for 24 h. (a) BF electron micrograph. (b) SADP of austenite matrix. The foil normal is [011].

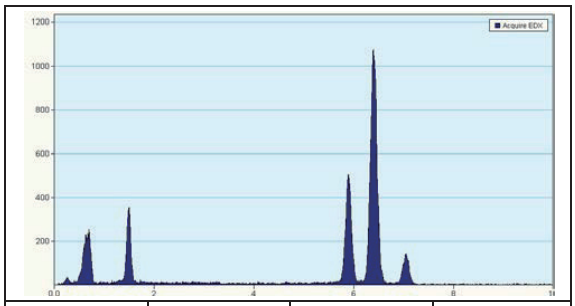

Mn	Al	C	Fe
16.9 wt%	9.0 wt%	0.9 wt%	bal

(a)

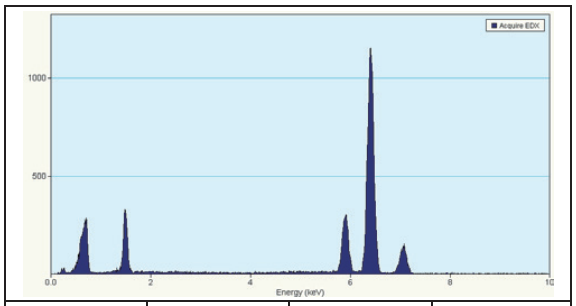

Mn	Al	C	Fe
27.2 wt%	9.0 wt%	1.7 wt%	bal

(b)

Fig. 12. (Color online) EDS spectra obtained from the austenite matrix of Fe-15Mn-10Al-1.0C alloy. (a) EDS spectrum of austenite matrix under the as-quenched condition and (b) EDS spectrum of the austenite matrix aged at 750 °C for 24 h.

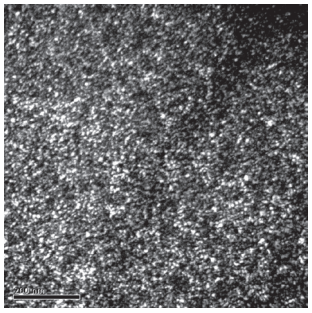

(a)

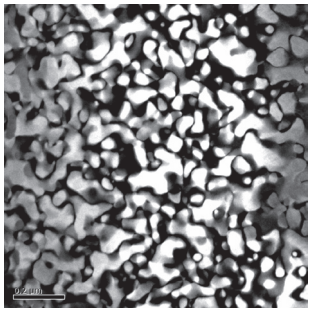

(b)

Fig. 13. TEM images of the Fe-15Mn-10Al-1.0C alloy aged at 750 °C for 24 h. DF electron micrographs of (a) the (111) $D0_3$ phase and (b) the (200) $D0_3$ and (100) B_2 phases.

Figure 13(a) is the DF electron micrograph of the $D0_3$ phase within the ferrite mixture, showing the existence of a tiny $D0_3$ ordered phase. Figure 13(b) is the DF electron micrograph of the $D0_3$ and B_2 phases, showing the existence of the B_2 phase. This microstructure is similar to that under the as-quenched condition. Experimental results indicated that when the Fe-15Mn-10Al-1.0C alloy was aged at 450 to 750 °C, the ordering phase transformation of $\alpha \rightarrow B_2 \rightarrow \alpha + D0_3$ occurred within the ferrite region. The transition temperature of the $B_2 \rightarrow \alpha + D0_3$ ordered transformation was found to be within the narrow range of 550–600 °C, which was quite different from the $\alpha \rightarrow B_2 \rightarrow \alpha + D0_3$ transition observed in the Fe-Mn-Al-C alloy by other researchers.

4. Conclusions

1. When the Fe-15Mn-10Al-1.0C alloy was aged at 450 °C for 24 to 72 h, the growth of the $D0_3$ ordered phase within the ferrite region revealed stable ($\alpha + D0_3$) phases with different morphologies within the ferrite region. Additionally, well-grown and newly precipitated

$(Fe,Mn)^3AlC_X$ carbides with L'12 crystal structures with different morphologies could be observed within the austenite matrix.

2. When the Fe-15Mn-10Al-1.0C alloy was aged at 650 ℃ for 24 h, the phase decomposition of $\gamma \rightarrow \kappa' + B_2$ could be observed on the austenite grain boundary. It is worth noting that the $\gamma \rightarrow \kappa' + B_2$ transformation was quite different from the $\gamma \rightarrow \alpha + \kappa'$, $\gamma \rightarrow \kappa' + D0_3$, and $\gamma \rightarrow \kappa' + \beta$-Mn transformations observed by other researchers.
3. When the Fe-15Mn-10Al-1.0C alloy was aged at 450 to 750 ℃, the ordering phase transformation of $\alpha \rightarrow B_2 \rightarrow \alpha + D0_3$ occurred within the ferrite region. The transition temperature of the $B_2 \rightarrow \alpha + D0_3$ ordered transformation was found to be within the narrow range of 550–600 ℃, which was quite different from the $\alpha \rightarrow B_2 \rightarrow \alpha + D0_3$ transition observed in the Fe-Mn-Al-C alloy by other researchers.

References

1 C. N. Hwang, C. Y. Chao, and T. F. Liu: Scr. Mater. **28** (1993) 263.
2 C. S. Wang, C. N. Hwang, C. G. Chao, and T. F. Liu: Scr. Mater. **57** (2007) 809.
3 C. C. Wu, J. S. Chou, and T. F. Liu: Metall. Trans. A **22** (1991) 2265.
4 Y. Kimura, K. Handa, K. Hoyashi, and Y. Mishima: Intermetallics **12** (2004) 607.
5 Inoue, T. Minemure, A. Kitamura, and T. Masumoto: Metall. Trans. A **12** (1981) 1041.
6 C. S. Wang, C. N. Hwang, C. G. Chao, and T. F. Liu: Scr. Mater. **57** (2007) 809.
7 G. Frommeyer, H. J. Habrock, J. E. Wittig, J. Geenen, and M. Kreuss: Scr. Metall. **24** (1990) 51.
8 Y. L. Lin and C. P. Chou: Scr. Metall. **28** (1993) 1261.